Lattice Imperfections of Energetic Materials Measured by X-ray Diffraction

Final Technical Report

by
Walter Engel, Michael Herrmann
January 2001

United States Army
EUROPEAN RESEARCH OFFICE OF THE U.S. ARMY
London, England
Contract Number: N68171-99-M-6474
August 1999 – August 2000
R&D 8678-CH-01S

Contractor:
Fraunhofer Institut für Chemische Technologie
Group for Applied X-ray Diffraction
J.-v.-Fraunhofer-Str. 7
D-76327 Pfinztal / Germany
Principal Investigator: Dr. Walter Engel

The Research reported in this document has been made possible through the support and sponsorship of the U.S. Government through its European Research Office of the U.S. Army.

REPORT DOCUMENTATION PAGE

Form Approved
OMB No. 0704-0188

1. AGANCY USE ONLY (Leave blank	2. REPORT DATE	3. REPORT TYPE AND DATES COVERED
	February 20th 2001	Final Tecnical Report

4. TITLES AND SUBTITLES
Lattice Imperfections of Energetic Materials measured with X-ray Diffraction

5. FUNDING NUMBERS
C = N68171-99-M-6474

6. AUTHOR(S)
Dr. Walter Engel, Dr. Michael Herrmann

7. PERFORMING ORGANIZATION NAME(S) AND ADDRESS(ES)
Fraunhofer Institut für Chemische Technologie
Joseph-von-Fraunhofer-Str.7
D-76327 Pfinztal (Berghausen) / Germany

8. PERFORMING ORGANIZATION REPORT NUMBER

9. SPONSERING/MONITORING AGENCY NAME(S) AND ADRESS(ES)
European Research Office of the U.S. Army
London England

10. SPONSERING/MONITORING AGENCY REPORT NUMBER

11. SUPPLEMENTARY NOTES

12a. DISTRIBUTION/AVAILABILITY STATEMENT
Public available

12b. DISTRIBUTION CODE

13. ABSTRACT (Maximum 200 words)
The mechanical sensitivity is an important issue for energetic materials and explosives, which has been discussed as a function of lattice defects originated during crystallization. However, hitherto a conclusive correlation was not achieved, because the quantitative measurement of defects is difficult. An approach is made to quantify defects in energetic materials with X-ray diffraction.
Samples of HMX were crystallized under varying conditions yielding different defect concentrations. The samples are investigated with X-ray diffraction, SEM, and the densities and the mechanical sensitivities were measured.
The SEM delivered information for the characterization of surface defects. Quantitative results were obtained by measurements of the density and the mechanical sensitivity. Both delivered significant deviations of the different HMX samples.
X-ray diffraction patterns of the samples were measured with different diffraction geometries, and the widths of diffraction peaks were determined. The data were evaluated with Williamson Hall plots revealing the micro strain for each sample.
The seed project shows that X-ray diffraction is capable for detecting qualities of coarse crystals, when suited measuring systems are applied. Moreover, the correlation of micro strain and mechanical sensitivities gives an idea, how far lattice imperfections influence macroscopic properties of energetic materials. The encouraging results give rise for further, refined investigations with an extended variety of crystallization conditions.

14. SUBJECT ITEMS
Lattice defects, Energetic materials, Sensitivity, X-ray Diffraction

15. NUMBER OF PAGES
28

16. PRICE CODE
$9,842.00

17. SECURITY CLASSIFICATION OF THIS REPORT	18. SECURITY CLASSIFICATION OF THIS PAGE	17. SECURITY CLASSIFICATION OF ABSTRACT	20. LIMITATION OF ABSTRACT
unclassified	unclassified	unclassified	

Summary

The mechanical sensitivity is an important issue for energetic materials and explosives, which has been discussed as a function of lattice defects originated during crystallization. However, hitherto a conclusive correlation was not achieved, because the quantitative measurement of defects is difficult. An approach is made to quantify defects in energetic materials with X-ray diffraction and to correlate the results with macroscopic properties.

12 samples of HMX were crystallized under varying conditions yielding different defect concentrations. The samples are investigated with X-ray diffraction, SEM, and the densities and the mechanical sensitivities were measured.

The SEM delivered information for the characterization of surface defects and morphology, but a quantitative detection is difficult, as the method is based on small arbitrarily selected parts of the sample. Quantitative results were obtained by measurements of the density and the mechanical sensitivity. Both delivered significant deviations of the different HMX samples.

X-ray diffraction patterns of the samples were measured with different diffraction geometries, and the widths of diffraction peaks were determined. The data were evaluated with Williamson Hall plots revealing the micro strain for each sample.

The seed project shows that the method is capable for detecting qualities of coarse crystals, when suited measuring systems are applied. Moreover, the correlation of micro strain and mechanical sensitivities gives an idea, how far lattice imperfections influence macroscopic properties of energetic materials.

The encouraging results give rise for further, refined investigations with an extended variety of crystallization conditions. Additionally, more detailed characterizations of imperfections in special energetic ingredients as HMX or CL20 should be started.

List of keywords

Energetic materials, lattice defects, micro strain, X-ray diffraction, sensitivity

Contents

1 Introduction

Lattice defects play an important role in material science, as they influence material properties. Well known examples are the electric properties of semi-conductors or the hardening of steel, which both depend strongly on the amount of guest or foreign atoms in the host lattice. Besides, defects like vacancies, interstitials, dislocations, misfits or inclusions interrupt the periodicity of crystallographic structures resulting in local or micro strain. The strained areas are discussed to build nuclei for phase transitions and decompositions or cause hot spots in energetic materials. Besides, dislocations can glide easily through crystals as shown in Fig. 1 and therefore increase the plasticity [Bohm 1995].

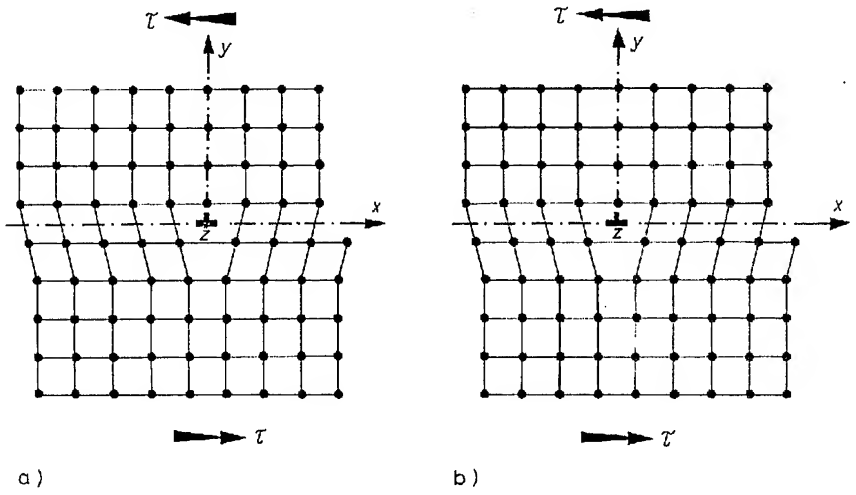

Fig. 1: Gliding of an edge dislocation through a lattice, schematically [Bohm 1995]

As the mechanical sensitivity is an important issue for energetic materials and explosives, it has been discussed as a function of lattice defects originated during crystallization. However, a conclusive correlation was hitherto difficult to achieve. Therefore an approach is made to quantify defects in energetic materials with X-ray diffraction and correlate the results with macroscopic properties.

2 Investigation of Lattice Defects

The methods used for the investigation of lattice defects are classified into direct and integral methods. Direct methods as Scanning Electron Microscopy SEM, Transmission Electron Microscopy TEM and High Resolution Electron Microscopy investigate small areas that are not representative for the sample. Besides, the preparation of the samples is time consuming and may induce defects. If one is aware of these limitations, SEM can be used for detecting coarse defects on the surface, TEM yields good results about defects in the bulk, and the High Resolution Electron Microscopy is even able to reproduce atomic structures.

In contrast to direct methods integral methods like the measurement of densities or thermodynamic values deliver data, which are representative for a sample. In the case of density it is assumed that defects like guest atoms or inclusions act as dilatation centers that decrease densities as vacancies do. The most meaningful measurement of such inhomogenities, however, is based on their influence on diffraction phenomena, especially in the case of X-ray diffraction [Bohm 1995].

The theory for the investigation of defects by means of X-ray Diffraction has been described in literature [Klug, Alexander 1974; Warren, Averbach 1949, 1950; Delhez et al. 1988, Langford 1988]. The method is well established in metallurgy, and special investigation methods were developed for high symmetry materials [Wilkens 1970; Krivoglaz et al. 1983; Klimanek, Kuzel, 1988, 1989; Klemm, Klimanek 1983]. Unfortunately no major efforts were made to apply the fundamental approach of Warren and Averbach to energetic materials with their lower symmetries.

As described by the kinematic theory and the Bragg's law, periodic structures of crystals diffract monochromatic X-rays at discrete diffraction angles. Therefore an ideal scan of the X-ray intensities versus diffraction angle should deliver sharp diffraction lines. In real measurements no sharp lines are observed, as geometric and sample effects broaden the lines, so that peak profiles have to be evaluated.

The superposition of a geometric and a sample profile is described by the convolution

$$h = g*f$$

where h is the measured, g is the geometric and f is the pure sample profile. As all information about the sample is included in the pure sample profile, its determination is one of the first tasks, if strain shall be determined absolutely. For relative investigations the measured profile may be evaluated without separating the sample profile, when geometric influences can be assumed constant.

As both, micro strain and particle size, broaden profiles the next task includes separating these effects by the method of Warren Averbach [1950] or the Williamson Hall plot [1953]. Both methods are based on the fact, that the peak broadening caused by micro strains depends on the order of the reflection, whereas broadening caused by small particles is independent of the order.

Williamson and Hall assume a strain distribution with an integral breadth ξ resulting in a line broadening described by $\beta_s = 2\xi\tan\theta$ with the Bragg angle θ. In the reciprocal lattice follows with $\beta^* = (\beta/\lambda)\cos\theta$ and $d^* = (2/\lambda)\sin\theta$

$$\beta^*_s = \xi d^*$$

where d^* is the distance between the reciprocal lattice point and the origin of the lattice and λ is the wavelength.

Small particles with a mean particle size t broaden profiles according to

$$\beta_p = \lambda/(t\cos\theta)$$

and in the reciprocal space to

$$\beta^*_p = 1/t$$

which is independent from d^*.

If both, particle size and strain broadening, are considered then the width can be approximated by adding the partial widths of strain and particle size. Plotting β^* versus d^* in the Williamson Hall plot delivers then a straight line with the slope ξ and an intercept with the y-axis at 1/t, if the widths are additive as in case of Cauchy profiles. In case of Gauss profiles, where the widths are not additive, a curve results with the slope ξ at higher values of d^* and an intercept at 1/t.

3 Experimental Details and Evaluation

3.1 Sample Preparation

β-HMX from Dyno Industrier with a purity of 98,6 % was solved in 900 g hot propylene carbonate (PC). The solutions were cooled from 75 to 5 °C with different cooling rates, resulting in cooling intervals of 2, 4, 6, 10 and 14 h. Beside the cooling rates the rotation of the stirrer was varied between 150 and 400 min^{-1}. The crystallization conditions of the samples are summarized in Tab. 1.

The crystallization procedures delivered coarse crystals with a size not well suited for X-ray diffraction measurements. However, grinding the particles to smaller particle sizes had to be avoided, as the procedure can create defects by itself.

Beside the crystallized batches the starting material "orig" and ground HMX "Techn" were used for the measurements.

3.2 X-ray Diffraction (XRD)

3.2.1 XRD Systems

The quantitative strain analysis as described in Chapter 2 is based on peak profile analysis, especially the measurement of the broadening of diffraction peaks. Therefore measuring systems are needed, with a minimal geometrical peak broadening by itself, combined with reasonable count rates. Difficulties are expected with the relatively large crystals obtained by crystallization procedures, considering poor orientation statistics or uneven sample surfaces as demonstrated in Fig. 2. Such effects are assumed causing split or shapeless profiles and therefore hindering peak profile analysis.

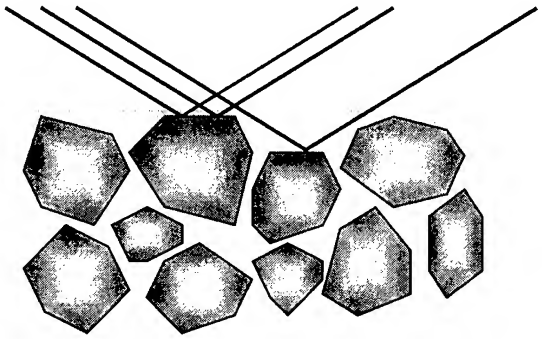

Fig. 2: Uneven surface caused by relatively large crystals in polycrystalline samples

A crucial task of the project is the selection and adjustment of suitable X-ray systems taking into account the requirements described above. Therefore different measuring systems were tested equipped with modern optical components as Göbel mirror, Channel Cut monochromators, primary or secondary monochromators and with rotating sample holders.

The Göbel Mirror, a bent multilayer crystal, is an optical component for parallizing monochromatic X-ray radiation a shown in Fig. 3. In combination with channel cut monochromators, soller slits or a second Göbel mirror on the detector side, the parallel beam concept suppresses effects caused by displacements or uneven surfaces of samples, which is one of the major errors sources in X-ray diffraction. Asymmetric monochromators as the V5-Channel cut monochromators or so called V-Groove crystals work in such a system as beam compressors or expanders as shown in Fig. 4, schematically. Systems with rotating sample holders improve the orientation statistics.

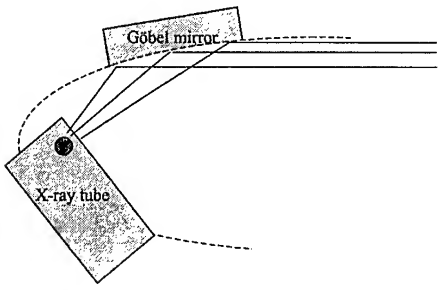

Fig. 3: Göbel mirror, schematically.
The mirror parallizes divergent X-ray radiation

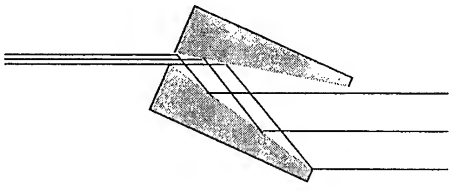

Fig. 4: V5-Channel cut monochrmator.
The monochromator expands or contracts parallel beams

Tests were performed with the following systems.

System 1: D5000/D8, Bragg-Brentano, no rotation

The conventional system consists of a Bragg-Brentano diffractometer D5000 or D8 of *Bruker AXS* equipped with a copper tube, scintillation counter, vertical Soller slits in incident and reflected beam, k_β-filter and flat specimen holder of the low temperature chamber TTK of *Paar Inc.*

System 2: D5000/D8, Debye-Scherrer, rotating capillary

The system consists of the diffractometer described above equipped, however, with a Debye-Scherrer device with rotating capillary and a secondary monochromator.

System 3: D5000/D8, Göbel mirror, rotation

The system consists of a Bragg-Brentano diffractometer D5000 or D8 equipped with a copper tube, Göbel mirror, secondary monochromator, scintillation counter, long horizontal Soller slit, vertical Soller slits in incident and reflected beam and k_β-filter.

System 4: Guinier, transmission, primary monochromator, rotating sample

The system consists of a diffractometer with transmission geometry equipped with a Johannson monochromator of *Huber* in incident beam and a position sensitive proportional counter (PSPC) of *Braun*. The vertical divergence of incident and diffracted beam was reduced by Soller slits to 1°. The samples were prepared on a rotating sample holder of *Huber*. The combination of PSPC and rotating sample holder is assumed to deliver better orientation statistics, compared to the systems described before.

System 5: V5-Channel-Cut

The system consists of a diffractometer equipped with Göbel mirror and asymmetric channel-cut monochromator in incident beam and a V5-Cannel Cut monochromator in diffracted beam.

3.2.2 Evaluation and Adjustment of XRD Systems

For the evaluation and adjustment of the measuring systems standard materials of Quartz and Silicon were measured with varying values of divergence and antiscattering slit. The Full Widths at Half Maximum (FWHM) of measured diffraction peaks were determined with the program EVA of *Bruker-AXS* and summarized in Tab. 2 and Tab. 3.

Normalized peak profiles measured with the Bragg-Brentano-diffractometer (D5000) of system 1, are shown in Fig. 5. Thin slits below 0,3 ° decrease the count rates, the profiles become noisier but not thinner. The profiles measured with a slit width of 1 ° are significantly broadened compared to the other measurements. With the slit width of 0,3 ° a peak width of 0,057 °2θ combined with a rate of 6877 counts per second (cps) was observed, which presents a reasonable resolution and count rate for recognizing additional peak broadening by sample effects. However, the system does not take into account effects caused by large crystals.

Applying the Debye Scherrer device or a Göbel mirror combined with a secondary monochromator of the systems 2 and 3, peak widths between 0,15 and 0,2 and between 0,1 and 0,12 °2θ were observed, respectively, which were more than twice the width than those measured with the conventional system. Additionally, the count rates of the systems are relatively low, so that these systems do not meet the requirements for a significant detection of micro strain.

Peak widths of 0,05 °2θ combined with high count rates near 3000 cps were measured with system 4 in transmission, which meets the requirements for the detection of micro strain.

Very thin peaks of 0,028 °2θ were measured with the system 5 withV5-channel cut monochromator, but the count rates slow down to 126 cps, resulting in noisy peak profiles or unreasonably long measuring times.

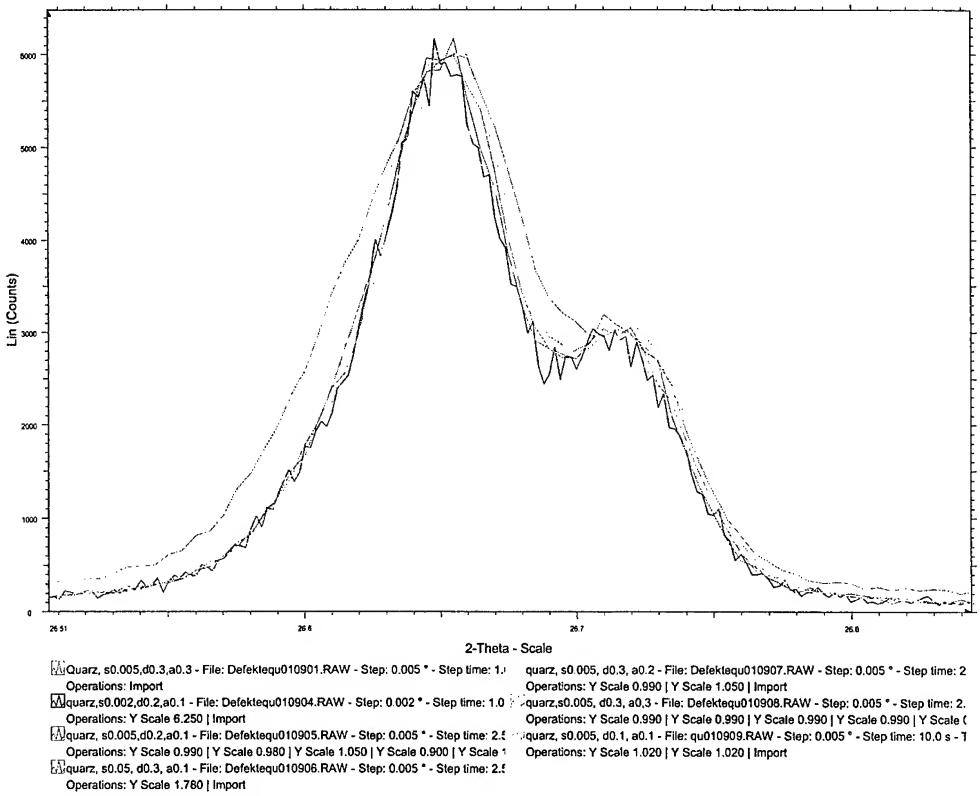

Fig. 5: X-ray diffraction line profiles of the (011)-reflection of Quartz measured with Bragg-Brentano Geometry under various conditions

3.2.3 XRD Measurements of HMX-Samples

Based on the results mentioned above HMX-samples were measured with

- *System 1: D5000/D8, Bragg-Brentano, no rotation,*
- *System 4: Guinier, transmission, primary monochromator, rotating sample and*
- *System 5: V5-Channel-Cut*

as summarized in Tab. 4.

3.2.4 Evaluation of HMX-Patterns

The full width at half maximum FWHM and integral peak widths of the diffraction pattern were determined with the program *EVA* of *Bruker-AXS*. The results were plotted in Williamson Hall plots as described in Chapter 2, and the resulting curves were fitted using $y=mx+b$. The slopes m of the fitted lines were used as relative values of mean micro strains ξ.

Additionally, the patterns measured with system 4 were evaluated by Rietveld analysis. This modern evaluation method calculates diffraction patterns based on models of the crystal structure. Fitting the calculated to a measured pattern in a second step delivers refined structure data as lattice parameters and crystal densities. Details of the method are described elsewhere [Rietveld 1969, Young 1995].

The data obtained by X-ray diffraction were compared with densities and mechanical sensitivities to find correlations of the micro strain with material properties.

3.3 SEM, Particle Size, Density and Mechanical Sensitivity

Pictures of the HMX-crystals were performed with a scanning electron microscope. A classification of sample properties seen in the SEM pictures is attempted, when the pictures were checked through for different types, and the defect concentrations and the particle sizes were estimated. Values between 0 and 3 were assigned to defect types, where 0 denotes a low and 3 a high defect density.

The particle size distributions were determined by laser diffraction spectroscopy with the "Mastersizer" of Malvern Instruments with a measuring range of 0,05 -3500 µm.

The densities were determined with the gas pycnometer "Ultrapycnometer 1000" of Quantachrome. The system measures the particle volume and mass, which is used to calculate the density.

According to BAM the mechanical sensitivities against impact and friction were determined with drop hammer and friction tests, respectively.

4 Results

4.1 X-ray Diffraction Measurements

The results are based on the diffraction patterns measured with 3 systems with the samples summarized in Tab. 4. The profiles recorded with the different measurement systems are discussed below. The calculated Full Widths at Half Maximum (FWHM) were used for preparing Williamson-Hall plots, see Fig. 9. The plots allow the separation of the peak broadening caused by lattice defects/micro strain and small particle sizes. The results are found in Tab. 5.

The diffraction patterns measured with the Guinier measuring system no. 4 with peaks nicely shaped above a low background encouraged us to attempt an evaluation procedure that is not included in the statement of work of the project. Rietveld refinement, which requires reasonably measured peak intensities, was used for the evaluation of the diffraction patterns. It delivers the elementary cell parameters, which allow the calculation of the cell volumes and of its densities provided the number of formula units in the elementary cell is known. The calculated densities are included in Tab. 5, which can be used for a correlation with the lattice defects/micro strain.

Measured Peak Profiles

Comparing the measured X-ray patterns with the ICDD powder diffraction files identifies β-HMX in the samples confirming the morphologic conclusions based on the SEM results.

Fig. 6 to Fig. 8 show the (001) reflections of HMX measurements with the measuring systems 1, 4 and 5. With the system 1, D5000/D8, the X-ray reflections in Fig. 6 are significantly shifted against each other, split or broadened, which is presumably caused by poor orientation statistics and uneven sample surfaces. The measurements confirm the assumption, that large crystals may hinder the evaluation of diffraction patterns measured with system 1, D5000/D8.

The Guinier measurements with system 4, transmission geometry, delivered well formed profiles and small peak shifts as shown in Fig. 7. System 4 is therefore well suited to overcome the problems raised by large crystals. With System 5, Göbel mirror and V5-channel-cut monochromator, the peak shifts are also strongly reduced in Fig. 8, indicating that difficulties with large crystals are overcome However, especially annoying are split peaks and low count rates, as a profile fit is difficult with such data. All in all, the measurements with the systems 4 and 5 confirm the improvement concerning the problems with the large crystals.

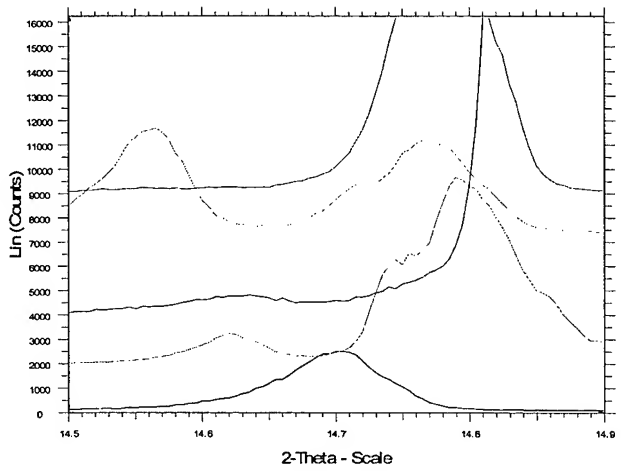

Fig. 6: (011) reflection of HMX measured with the conventional geometry on a D8 diffractometer (system 1)

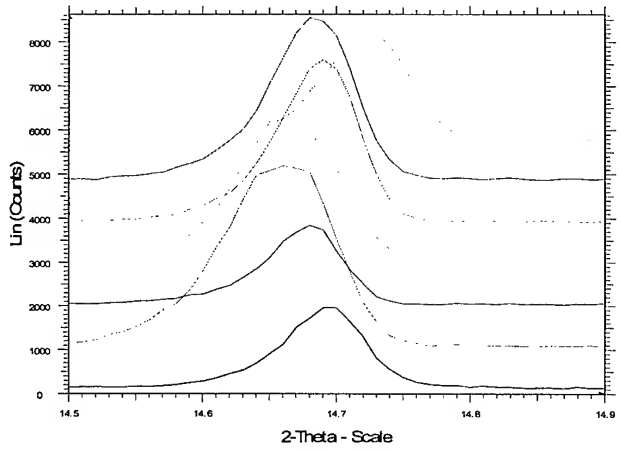

Fig. 7: (011) reflection of HMX measured with transmission geometry (system 4)

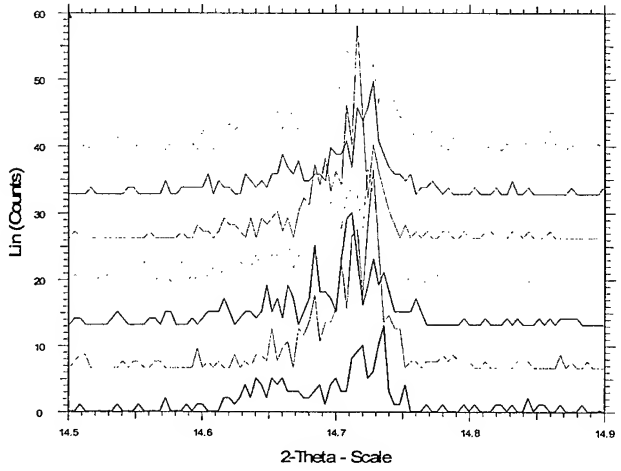

Fig. 8: (011) reflection of HMX measured with Göbel mirror and V5-channel-cut monochromator (system 5)

Williamson Hall-Plot

The relative micro strains determined by Williamson Hall-plots are summarized in Tab. 5. Fig. 9 shows selected plots and fitted lines of the samples V3, V6, V7 and the original sample measured with transmission geometry, where the slopes of the curves present the relative micro strain.

The lines fitted best with the data measured with the system 4 in transmission geometry, but with the conventional system 1 and the system 5 with Göbel mirror and V5-channel-cut monochromator also significant differences of the plotted lines were found indicating different crystal qualities.

The evaluation of the measurements with system 4 delivered slopes between 0,026 and 0,117, where the lowest micro strain represents the original sample and the highest values were found with the samples V2 and V3.

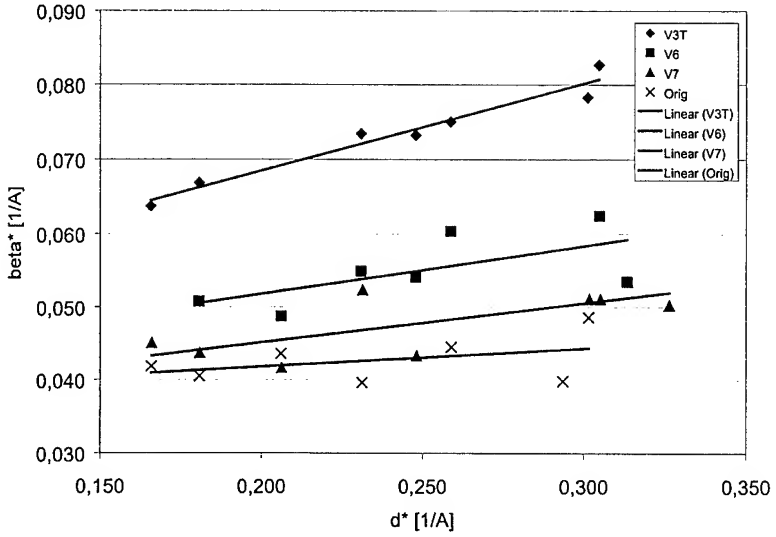

Fig. 9: Williamson-Hall-Plots of the samples V3, V6, V7 and the original sample, measured with transmission geometry

Rietveld Analysis

The lattice parameters a, b and c in Tab. 5 vary between 6,517 and 6,555, 10,997 and 11,061 and 8,678 and 8,7261,987 Å, respectively, resulting in calculated densities between 2,021 and 1,987 g/cm^3, found with the samples V2 and V3, respectively. The deviating parameters may present residual effects of large particles applying system 4 or residual strains of the HMX crystals.

4.2 Morphology and Surface Defects observed with SEM

The results of the investigations with SEM are summarized in Tab. 6 and selected pictures of defect types are shown in Fig. 10 to Fig. 19. The pictures show morphological features like corroded edges, uneven faces, holes, rounded particles, twins and agglomerates. The semi quanitative evaluation of these defects in Tab. 6 indicates a poor crystal quality of sample V9 and the ground sample "Technikum".

Fig. 10 shows well crystallized particles of the sample V2. The compact habit of the crystals agrees with the habit of β-HMX, found by former investigations. Besides, the sample includes porous particles (Fig. 11), which point to a poorer crystal quality.

Strongly corroded edges and surfaces were found in sample V9 as shown in Fig. 12. The sample showed also holes and apparently amorphous parts, resulting in a poor classification in Tab. 6. In contrast to sample V9, holes were also found in otherwise well crystallized particles of sample V20 (Fig. 13).

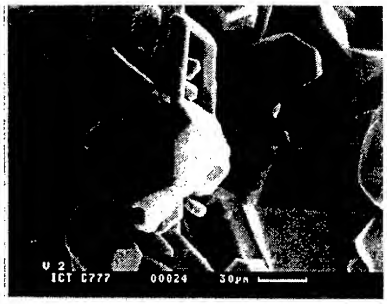

Fig. 10: Well crystallized particles of sample V2

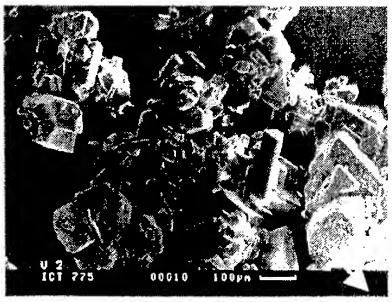

Fig. 11: Porous beside well crystallized particles of sample V2

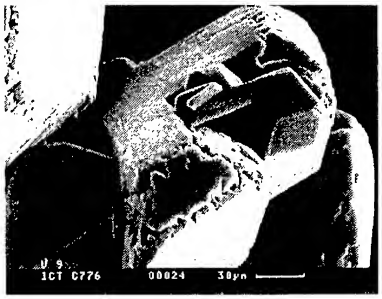

Fig. 12: Corroded crystals of sample V9

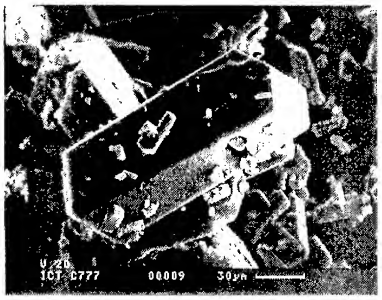

Fig. 13: Hole in well crystallized particle of sample V20

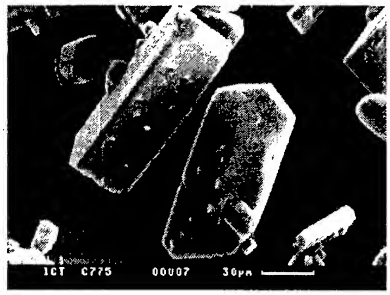

Fig. 14: Upgrowths or apparently intergrown particles of sample V1

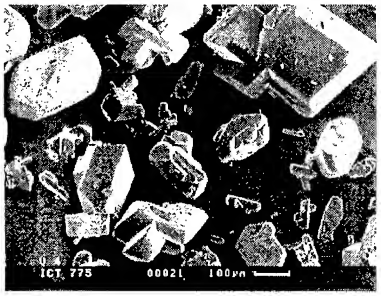

Fig. 15: Twin and intergrown crystals of sample V4

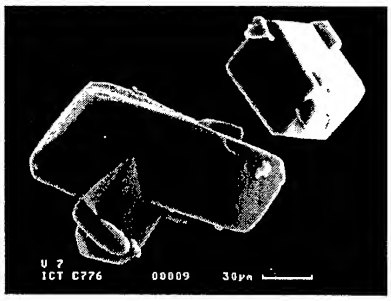

Fig. 16: Rounded twin of sample V7

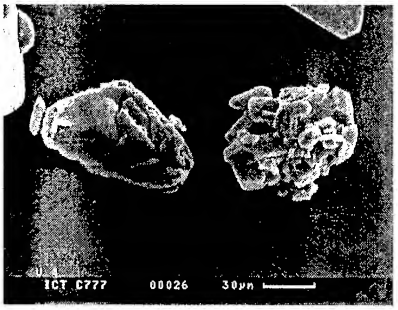

Fig. 17: Rounded, intergrown particle and agglomerate of sample V4

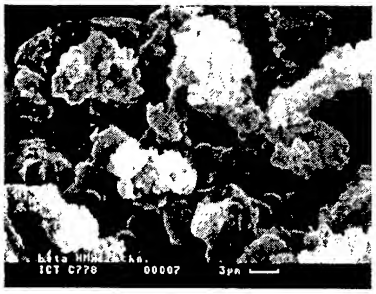

Fig. 18: Agglomerates of the ground sample (Technikum)

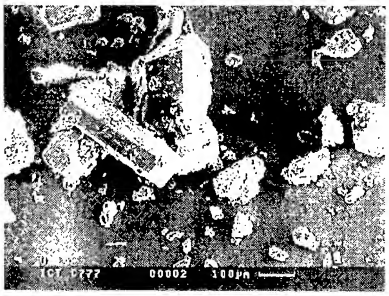

Fig. 19: Approximately bimodal particle size distribution of V19

Surfaces with upgrowths or apparently intergrown crystals were found in sample V1 (Fig. 14). Their origin presumably lies inside the host crystal. Intergrowths of larger crystals are presented by the twins of sample V7 (Fig. 15). The crystals of this sample also show rounded edges, which are presumably caused by the strongly rotating stirrer during the crystallization.

Besides the defects, different particle sizes and agglomerations are observed. Fig. 17 and Fig. 18 show the agglomeration of sample V4 and a ground sample, respectively. No crystal faces could be observed with the ground sample. The samples V3, V19 and V20 include major parts of fine material, which mostly settle down on major crystals. The approximately bimodal particle size distribution of sample V19 with particles of 100 - 500 µm together with 10 µm-particles is seen in Fig. 19.

4.3 Particle Size, Density and Mechanical Sensitivity

Densities, particle sizes and mechanical sensitivities against friction and impact are summarized in Tab. 7 and Tab. 8 and plotted in Fig. 20 to Fig. 23.

The densities of most samples lie in a narrow range between 1,889 and 1,895 g/cm^3. Significantly lower values of 1,843, 1,874 and 1,872 g/cm^3 were observed with the samples V2, V8 and V9, respectively.

The mean particle sizes of the crystallized samples range between 85 and 721 µm. Small particles were found with the samples V1 and V2 with 85 and 96 µm, large particles with the samples V3 and V19 with 633 and 721 µm, respectively. The particle sizes of the ground sample "Technikum" lie in the order of 5 µm, determined from Fig. 18.

The impact energies of the HMX sample lie between 4 and 7,5 Nm. The samples V3, V5, V42/2 and the ground sample look more sensitive against impact than the other samples, especially in contrast to the samples V2, V6, V7, V9, V19, V20 and V21 with the lowest sensitivities.

The pin loads of the friction tests lie between 72 and 96 N for all samples except the samples V2 and V3, where significantly higher values of 144 and 112 N were observed, respectively.

Amongst the crystallized samples, sample V2 shows an exceptional characteristic with a significantly low density, particle size and sensitivity against friction.

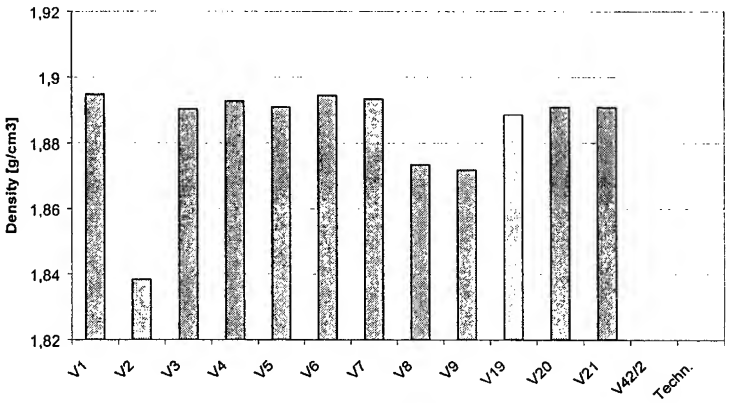

Fig. 20: Densities of the HMX samples;
The densities of the samplesV2, V8 and V9 are comparably lower

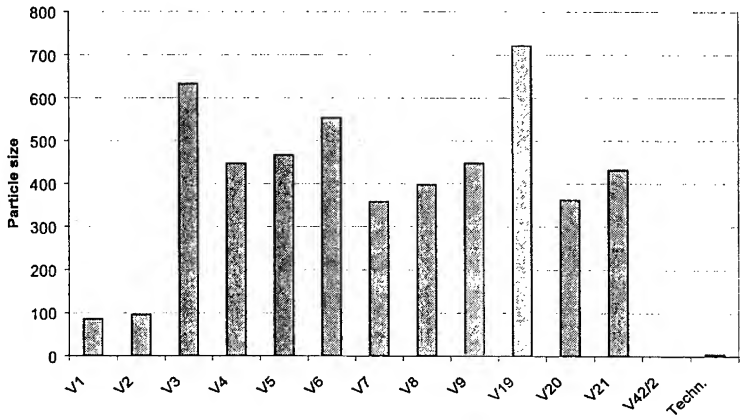

Fig. 21: Particle sizes of the HMX samples [µm];
The particle sizes of the samples V1 and V2 are comparable lower

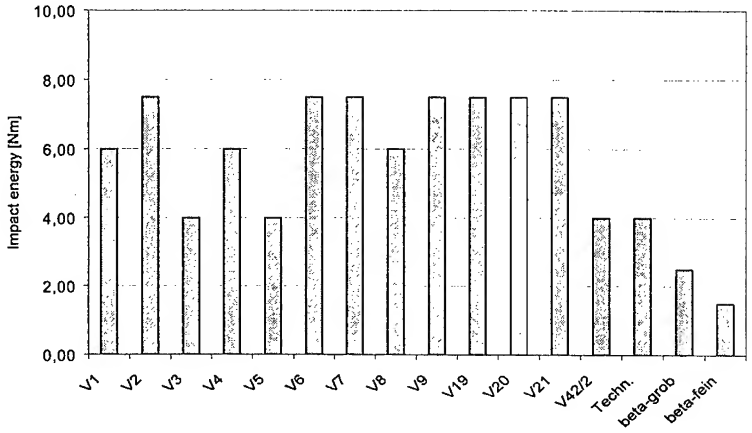

Fig. 22: Impact energy of the HMX samples, determined according to BAM

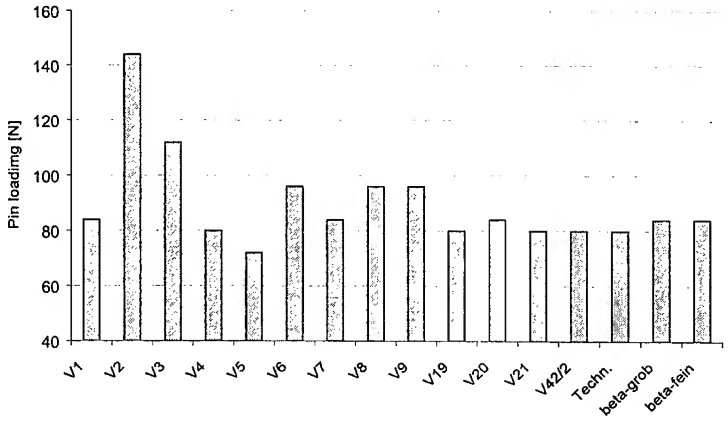

Fig. 23: Friction Sensitivity determined according to BAM

5 Correlation of Results and Discussions

In the former chapter values for a relative micro strain were measured by XRD and evaluated by Williamson-Hall-plots. The evaluation revealed significant differences of the micro strain of the samples. Now the question is raised, if the micro strain correlates with other measured properties of the samples like impact and friction sensitivities, densities, particle sizes, lattice parameters, crystal qualities seen in the SEM pictures or crystallization parameters.

The correlation with impact and friction is highly interesting in the field of energetic materials, because sensitivities and safety aspects must always be taken into account. Another interesting correlation concerns lattice defects/densities, which could answer the question, if its influence on material properties is so severe that it influences the measured densities. The correlation with particle sizes and crystallization parameters would encourage attempts to crystallize less sensitive products. Finally it is interesting, if micro strain and lattice defects can already be deduced from the regular and irregular particles seen with SEM.

Therefore plots of the results obtained with the different investigation methods plotted against each other are presented in the annex under Chapters 9.1 and 9.2, which give a general idea of the results. Besides, selected plots are shown and discussed in detail in the following presentation.

5.1 Mechanical Sensitivity

Plots of impact and friction sensitivities against micro strain are seen in Fig. 31 to Fig. 36 for the systems 1, 4 and 5. Fig. 24 shows a highly correlating pin load of the friction test, which increased significantly with the micro strain measured with system 4. The effect was also found with the conventional system 1 (Fig. 31) and in tendency with system 5 (Fig. 35).

The correlation gives rise for the hypothesis, that energetic materials could become more insensitive against friction with an increasing concentration of defects. Considering dislocations, which can migrate through crystals easily as shown in Fig. 1, the effect may be caused by an increased plasticity.

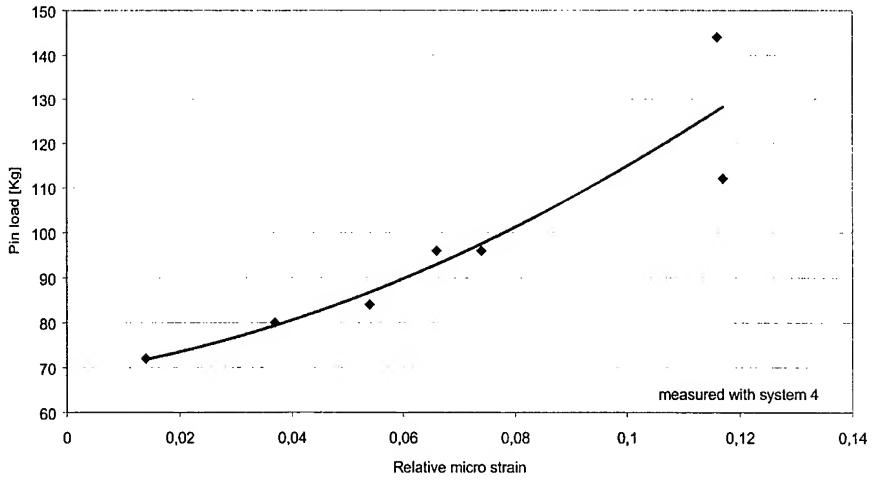

Fig. 24: Pin load of the friction test versus micro strain measured with system 4.
The correlation suggests, that increasing micro strain decreases the sensitivity against friction.

The plots of the impact energies against micro strain in Fig. 32, Fig. 34 and Fig. 36 revealed no significant correlation. Thus, the assumption that defects or micro strain increase the sensitivity against impact due to nucleation of hot spots was not confirmed. The plots, however, showed a relatively poor resolution of the impact test resulting in three values of the impact energy as shown in Fig. 25, which may explain the failing correlation.

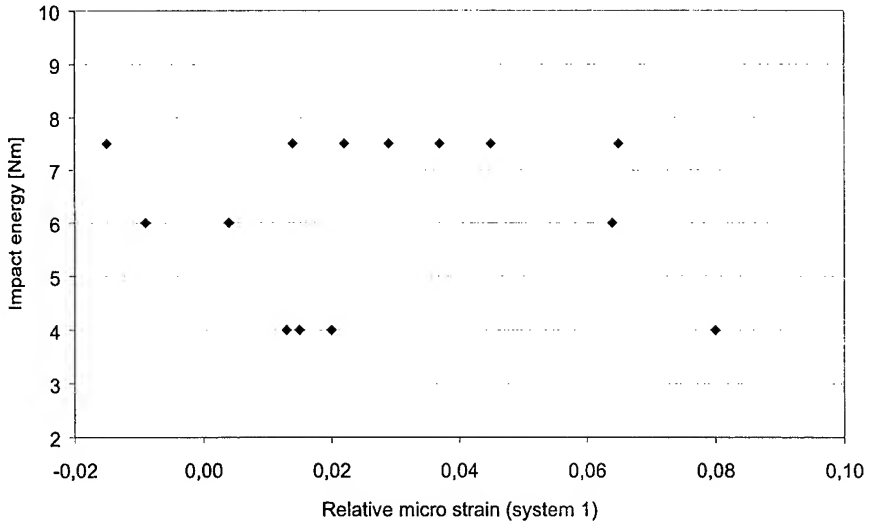

Fig. 25: Impact energy versus micro strain measured with system 1.

5.2 Density and Particle Size

No significant correlation was found by plotting the micro strain against the measured density in Fig. 37, Fig. 39 and Fig. 41. Amongst the plots of micro strain versus particle size the approximately identical plots obtained with system 4 and 5 (Fig. 26) and the trend of the plot obtained with system 1 point to a minimum micro strain at a particle size between 400 and 500 μm.

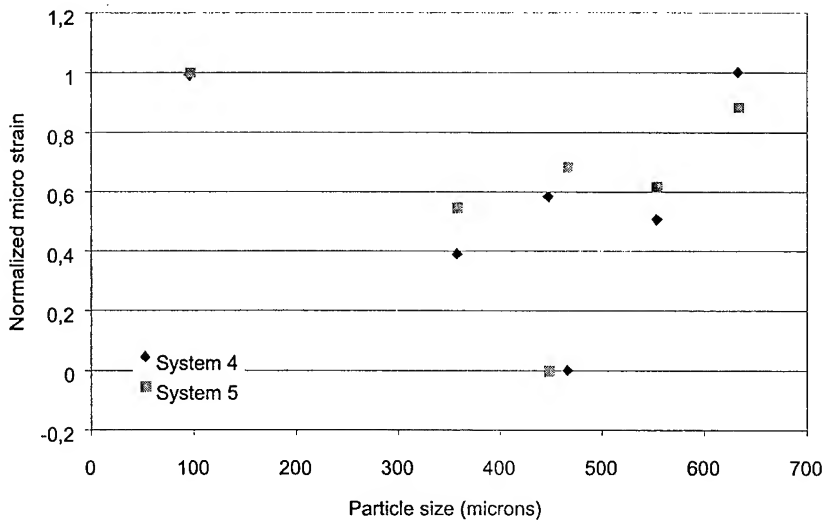

Fig. 26: Normalized micro strain measured with system 4 and 5 plotted against the particle size. The approximately identical plots point to a minimum micro strain at a medium particle size.

5.3 Lattice Parameters

Plots of micro strain versus lattice parameters from Rietveld analysis and lattice parameters versus particle size are shown in Fig. 43 to Fig. 48. The lattice parameters, represented in Fig. 27 by parameter a, show a minimum micro strain near an average value and increasing micro strain connected with any deviation from this average value. The results rise the question, if the deviations of lattice parameters from the average value represent residual strains of the crystals or if they originated by peak shifts caused by measurements with coarse crystals.

As the lattice parameters evaluated by Rietveld analysis correlate highly with the particle size (Fig. 28) two explanations of the effects seem possible.

- The crystals are exposed to a residual strain, which increases with larger crystals
- The residual effect of sample displacement of large crystals measured with the system 4 influence the evaluation with Rietveld analysis resulting in an apparent correlation of lattice parameters and micro strain.

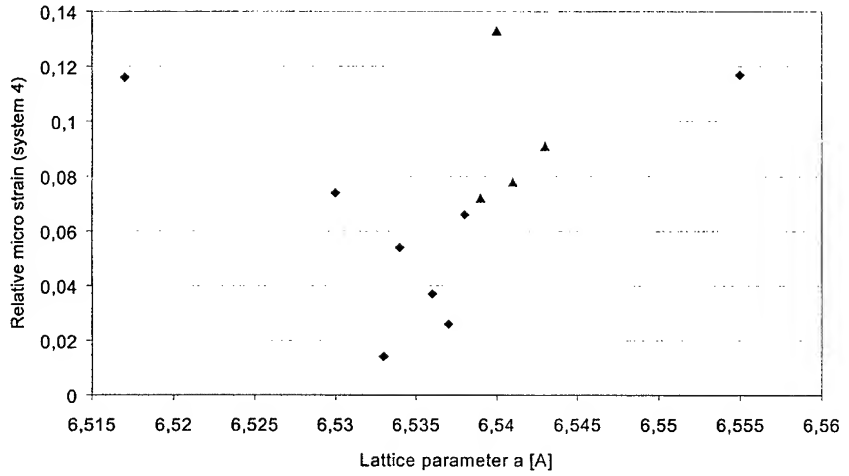

Fig. 27: Relative micro strain plotted against the lattice parameter a evaluated by Rietveld analysis.

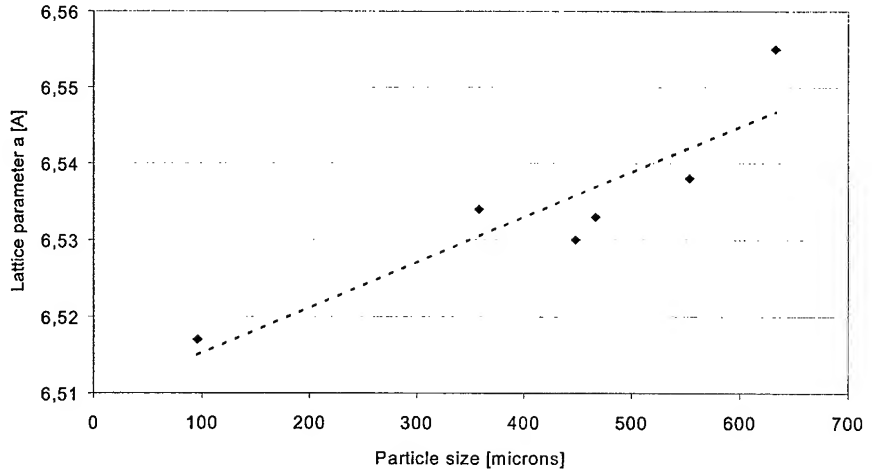

Fig. 28: Lattice parameter a plotted against the particle size.

5.4 SEM Pictures

A conclusive correlation of the qualities seen in the SEM pictures with the micro strain was not found.

5.5 Crystallization Parameters

Fig. 52 to Fig. 55 show plots of the micro strain measured with the different systems in dependence of the crystallization parameters stirrer frequency and cooling rate. The micro strain decreased, when the stirrer frequency was increased from 150 to 250 min^{-1}. The effect was found with all X-ray measuring systems. Stronger stirring resulted with frequencies above 250 min^{-1} resulted partially in increased or decreased micro strains as shown in Fig. 29.

Plotting the micro strain measured with diffraction system 1 against the cooling time in Fig. 30 shows, that the micro strain was increased when the cooling time was expanded from 2 to 4 or 6 h and decreased for longer cooling times. The results was partially confirmed by the results obtained with diffraction system 4 but contradicted with system 5. It should be mentioned in this context, that the reduced set of samples measured with the systems 4 and 5 do not present cooling times longer than 6 h.

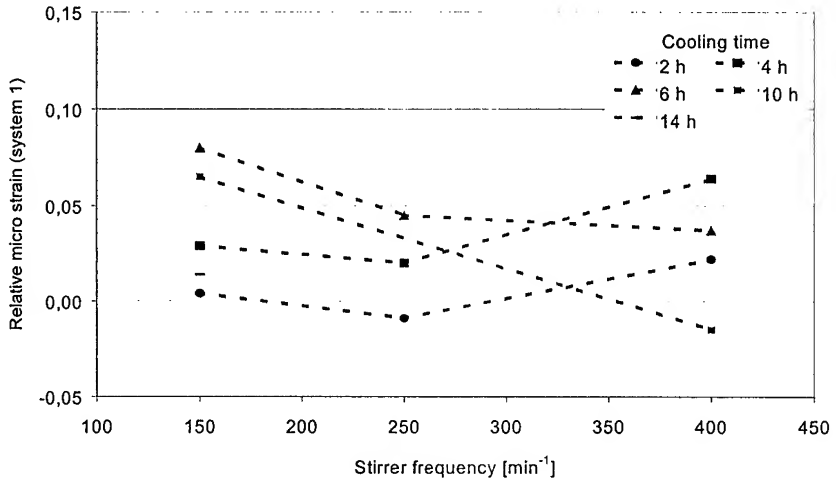

Fig. 29: Relative micro strain plotted against the stirrer frequency (system 1)

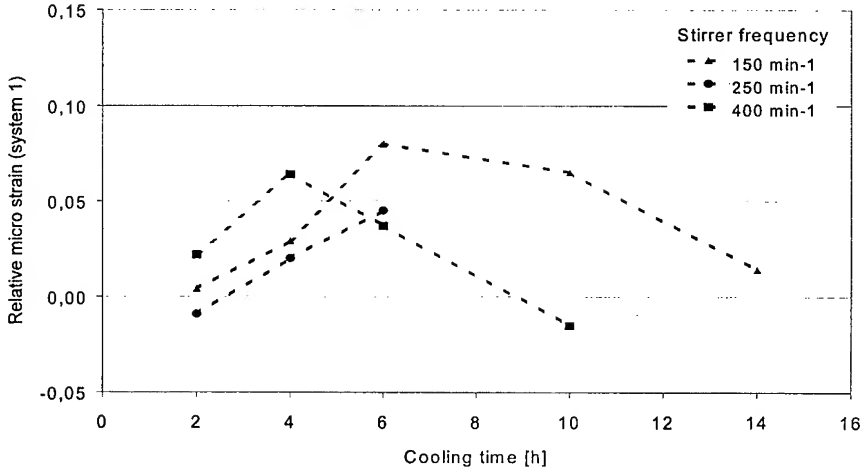

Fig. 30: Relative micro strain in dependence of the cooling time (system 1)

Considering the revolution of crystals by stirring combined with collisions of growing crystals with the stirrer or other particles, it is assumed that stronger or longer stirring induces a higher concentration of lattice imperfections. On the other hand, with longer cooling times, it is assumed that crystals have more time to grow with a more perfect habit and lattice. These ideas are not supported by the results. A conclusion could be, that the creation of lattice defects in HMX is related to more complex mechanisms.

6 Conclusions and Future Research Plans

The central issue of the project was the question, if X-ray diffraction can provide the tool for measuring micro strain and lattice defects. The results give a positive answer. It can be expected that micro strain can be measured quantitatively or at least semiquantitatively with X-ray diffraction.

The experiments, which were performed with different measuring systems, allow also a statement, which measuring systems are suited for the task. Conventional Bragg-Brentano-diffractometers are not suited, when coarser samples are included, which must not be ground to avoid creation of lattice defects. The displacement errors induced with the coarse material causes considerable peak shifts in the diffraction patterns.

When the diffractometer is equipped with a Göbel mirror, these difficulties are overcome. The additional combination with a channel-cut-monochromator could not yet meet our requirements. Obviously the narrow beam leaving the monochromator illuminates only few particles so that no smooth diffraction peaks are obtained. The potential of these systems, however, is considerable. It is conceivable that after a better adaptation to the problem such a system can be used.

The best results, however, were obtained with Guinier measurements with a rotating sample in transmission position. Obviously the system is not sensitive to problems caused by coarser material. Besides, the intensities are good so that the patterns can even be used for Rietveld evaluation.

The relative micro strain obtained with Williamson-Hall-plots revealed considerable differences between different samples. When the values were plotted against the measured impact and friction sensitivities of the samples, no correlation was observed with impact sensitivity as expected. A correlation, however, was found with the friction sensitivities. Surprisingly the sensitivity decreased with increasing micro strain/lattice defects.

Another correlation was found with the crystallization parameters cooling rate and stirring. The result gives rise to the hope that less sensitive crystals can be obtained by optimized crystallizing conditions.

Plotting the lattice parameters from Rietveld shows that high micro strain correlates with deviation from an average value. It can, however, not be excluded, that the deviations are caused by errors of the measurement of the peak positions, which lead then to errors of the lattice parameters.

Looking on the positive results it must, however, not be forgotten, that the data basis is still very small. Further investigations are recommended with broader number of samples, which were prepared under more differing crystallizing conditions. An optimization of the measuring conditions looks also promising. The procedure of using Williamson-Hall plots has worked fine. Nevertheless an attempt should be made using new features of advanced Rietveld evaluation programs. These programs allow fitting the parameters, which describe the peak broadening induced by micro strain. The potential of the method should justify further efforts.

7 Acknowledgement

We thank Dr. Herbert Göbel, Siemens München, for fruitful discussions and stimulation concerning modern X-ray optics and Göbel mirrors.

8 Literature

Bohm J., Realstruktur von Kristallen, Stuttgart: Schweizerbart, ISBN 3-510-65160-X, (1995)

Delhez R. de Keijser Th. H., Mittemeijer E. J., Langford J. I.; Size and Strain Parameters from Peak Profiles: Sense and Nonsense; Aust. J. Phys., **41**, 213-27 (1988)

Klemm V., Klimanek P.; Application of Lattice Parameter Measurements in X-ray Analysis of Elastic Distortion Due to Intersitial Atoms in Metals; Crystal Res. & Technol. **18**, K 112-115 (1983)

Klimanek P.; X-Ray Diffraction Line Profiles Due to Real Polycrystals; Mat. Sci. Forum Vols. **79-82**, 73-84 (1991)

Klimanek P., Kuzel R. Jr.; X-ray Diffraction Line Broadening Due to Dislocations in Non-Cubic Materials. I. General Considerations and the Case of Elastic Isotrpy Applied to Hexagonal Crystals; J. Appl. Cryst. **21**, 59-66 (1988)

Klug H.P., Alexander L.E.; X-Ray Diffraction Procedures, ISBN 0-471-49369-4, J. Wiley & Sons Inc., (1954)

Krivoglaz M. A., Martynenko O. V., Ryaboshapka K. P.; Influence of Correlation in Position of Dislocations on X-ray Diffraction by Deformed Crystals; Phys. Met. Metall., Vol. 55, 1-12, (1983)

Kuzel R. Jr., Klimanek P.; X-ray Diffraction Line Broadening Due to Dislocations in Non-Cubic Materials. II. The Case of Elastic Anisotropy Applied to Hexagonal Crystals; J. Appl. Cryst. **21**, 363-368 (1988)

Kuzel R. Jr., Klimanek P.; X-ray Diffraction Line Broadening Due to Dislocations in Non-Cubic Materials. III. Experimental Results for Plastically Deformed Zirconium; J. Appl. Cryst. **22**, 299-307 (1989)

Langford J. I., Delhez R., de Keijser Th. H., Mittemeijer E. J.; Profile Analysis for Microcrystalline Properties by the Fourier and Other Methods; Aust. J. Phys., **41**, 173-87 (1988)

Rietveld H. M.; A profile refinement method for nuclear and magnetic structures; J. Appl. Cryst. 2:65-71(1969)

Stokes A.R.; Proc. Phys. Soc. (London), A61, 382, (1948)

Warren B.E.; X-Ray Diffraction, Addision-Wesley, Reading, Massachusetts, 1969

Warren B.E., Averbach B.L.; The effect of Cold-Worked Distortion on X-Ray Patterns; J. Appl. Phys., Vol. **21**, 595-599, (1950)

Warren B.E.; Progress in Metal Physics **147**, 8 (1959)

Wilkens M.; The Determination of Density and Distribution of Dislocations in Deformed Single Crystals from Broadened X-Ray Diffraction Profiles; Phys. stat. sol. (a) **2**, 359 (1970)

Williamson G. K., Hall W. H.; X-ray Line Broadening from filed Aluminium and Wolfram; Acta Metall., Vol **1**, 22-31 (1953)

Young R. A.; The Rietveld Method; Int Union of Cryst., Oxford Sci. Publ., ISBN 0198559127, (1995)

9 Annex

9.1 Plots Related to Micro Strain or Lattice Parameters

9.1.1 Mechanical Sensitivity

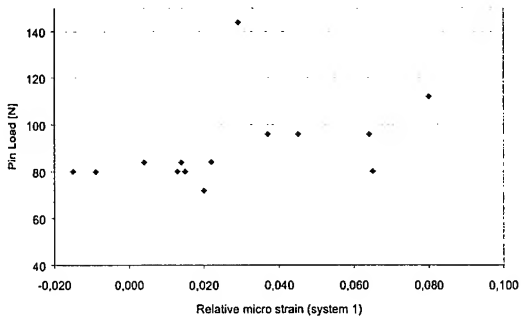

Fig. 31: Pin load plotted versus micro strain (system 1)

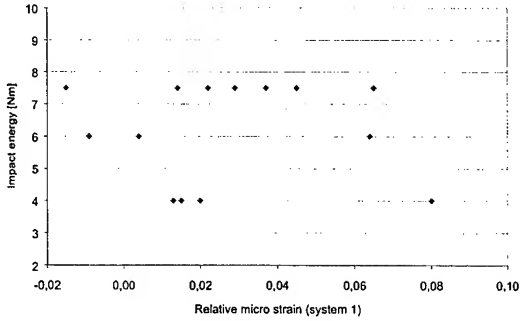

Fig. 32: Impact energy plotted versus micro strain (system 1)

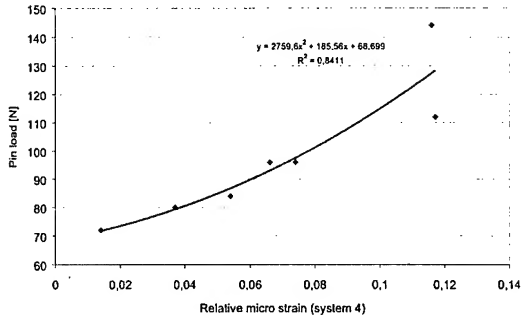

Fig. 33: Pin load plotted versus micro strain (system 4)

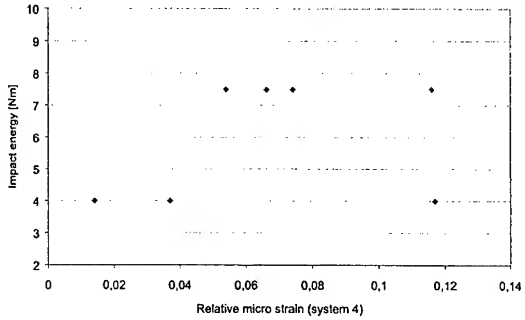

Fig. 34: Impact energy plotted versus micro strain (system 4)

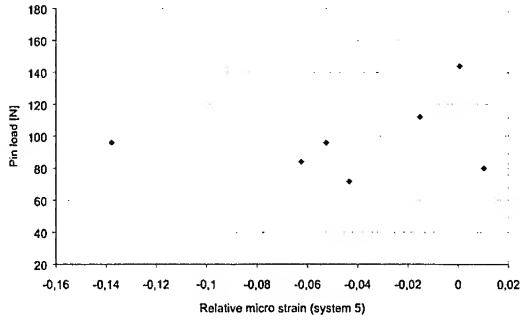

Fig. 35: Pin load plotted versus micro strain (system 5)

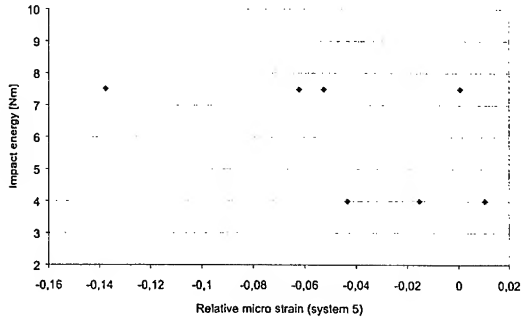

Fig. 36: Impact energy plotted versus micro strain (system 5)

9.1.2 Density and Particle Size

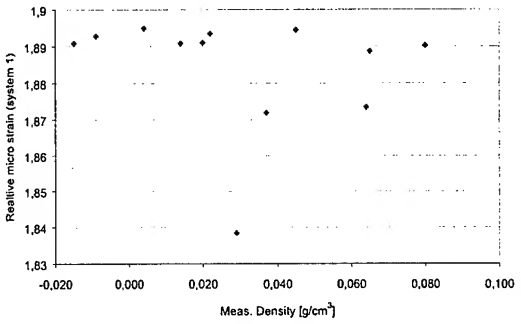

Fig. 37: Micro strain plotted versus meas. density (system 1)

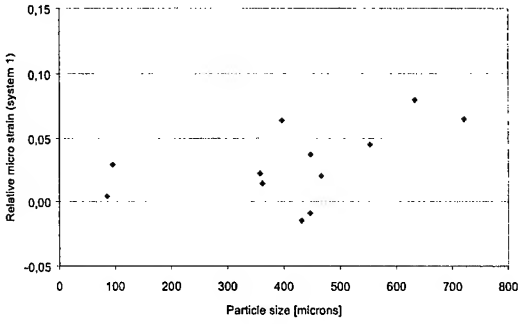

Fig. 38: Micro strain plotted versus particle size (system 1)

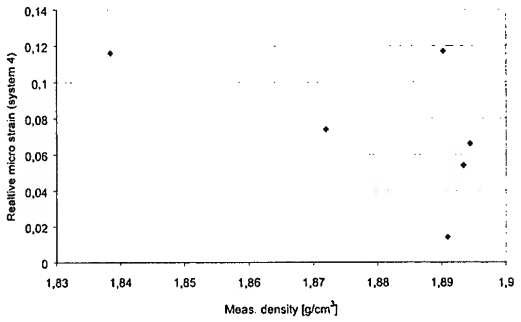

Fig. 39: Micro strain plotted versus meas. density (system 4)

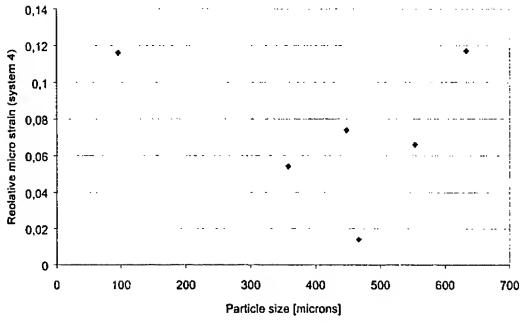

Fig. 40: Micro strain plotted versus particle size (system 4)

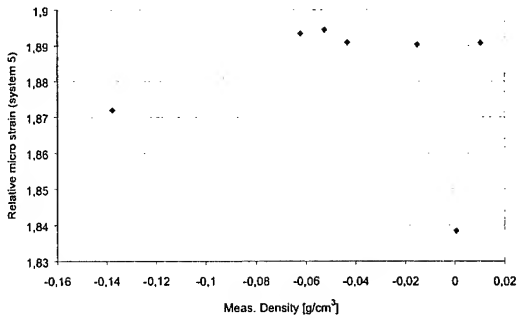

Fig. 41: Micro strain plotted versus meas. density (system 5)

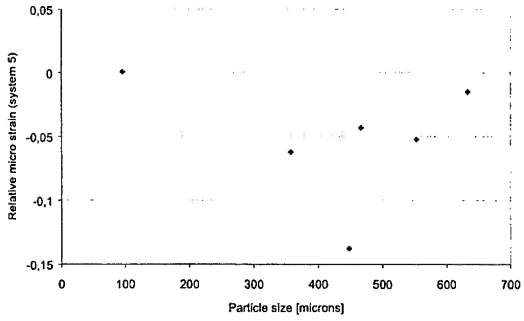

Fig. 42: Micro strain plotted versus particle size (system 5)

9.1.3 Lattice Parameters

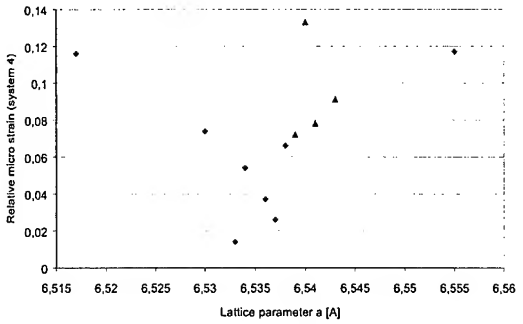

Fig. 43: Micro strain plotted versus lattice parameter a (system 4)

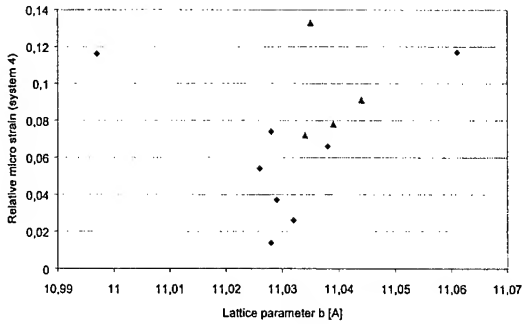

Fig. 44: Micro strain plotted versus lattice parameter b (system 4)

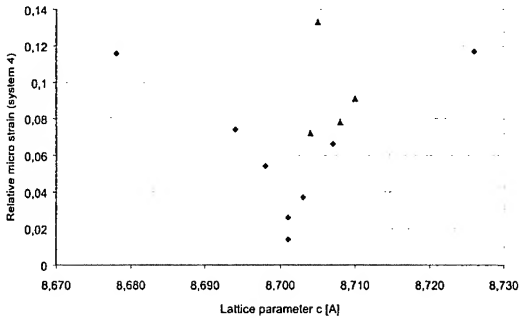

Fig. 45: Micro strain plotted versus lattice parameter c (system 4)

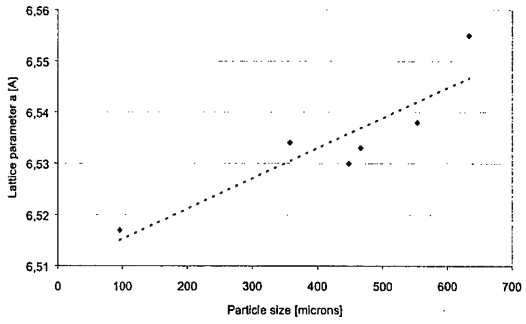

Fig. 46: Lattice parameter a plotted versus particle size (system4)

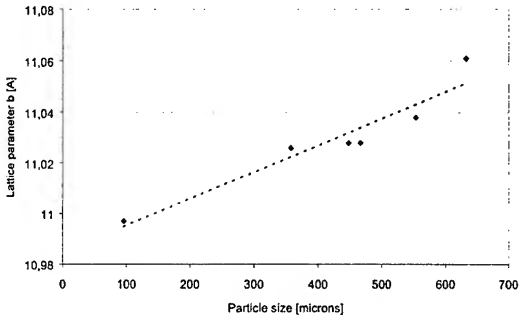

Fig. 47: Lattice parameter b plotted versus particle size (system4)

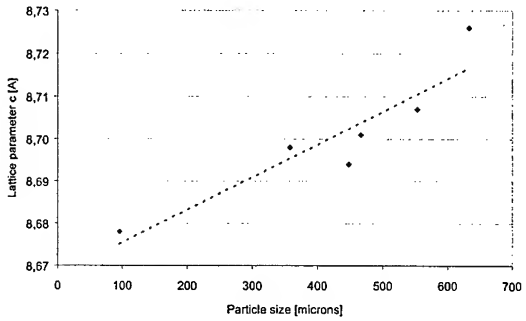

Fig. 48: Lattice parameter c plotted versus particle size (system4)

9.1.4 Williamson Hall Parameter b

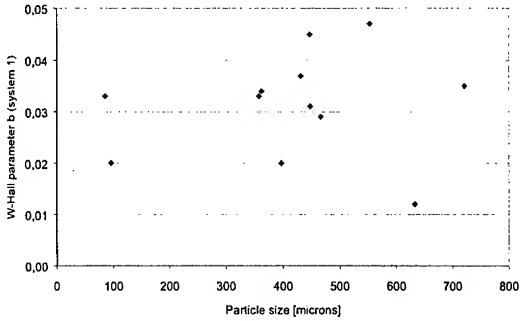

Fig. 49: W-Hall parameter b plotted versus particle size (system 1)

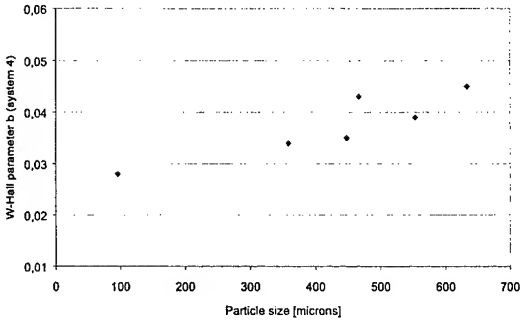

Fig. 50: W-Hall parameter b plotted versus particle size (system 4)

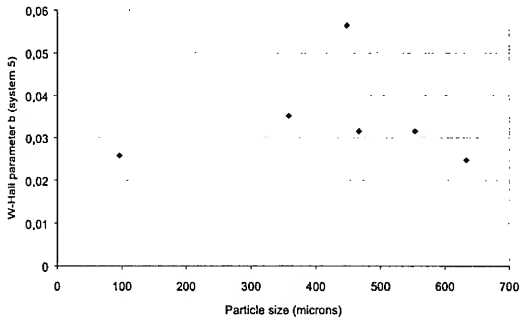

Fig. 51: W-Hall parameter b plotted versus particle size (system 5)

9.1.5 Crystallization Conditions

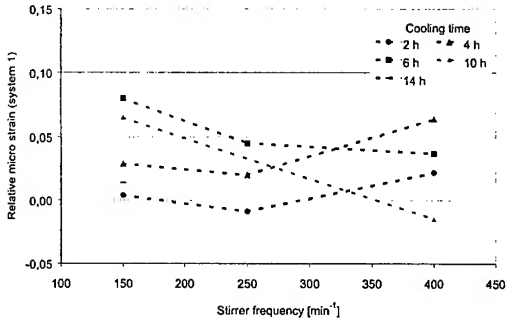

Fig. 52: Micro strain plotted versus stirrer frequency (system 1)

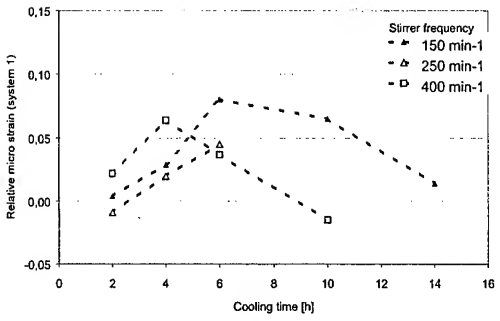

Fig. 53: Micro strain plotted versus cooling time (system 1)

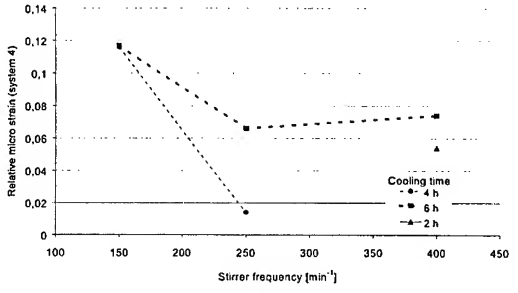

Fig. 54: Micro strain plotted versus stirrer frequency (system 4)

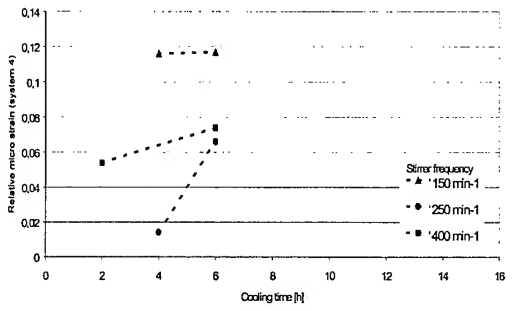

Fig. 55: Micro strain plotted versus cooling time (system 4)

9.2 Other Plots

9.2.1 Mechanical Sensitivity / Crystallization Conditions

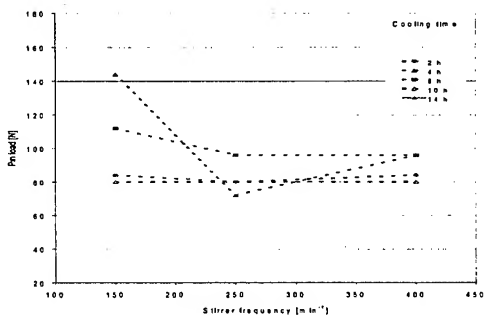

Fig. 56: Pin load plotted versus stirrer frequency

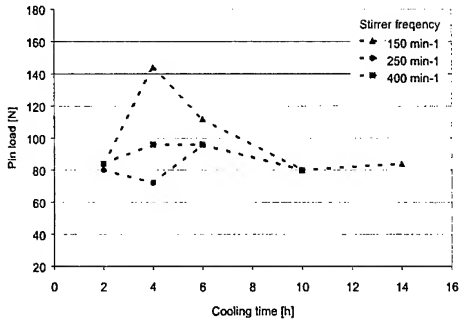

Fig. 57: Pin load plotted versus cooling time

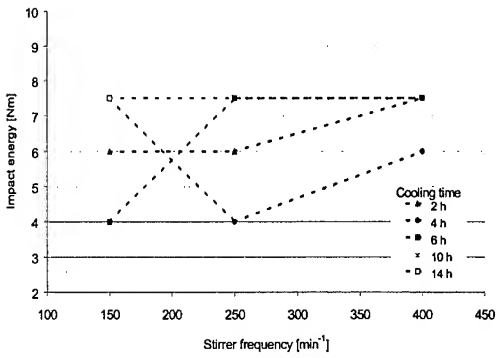

Fig. 58: Impact energy plotted versus stirrer frequency

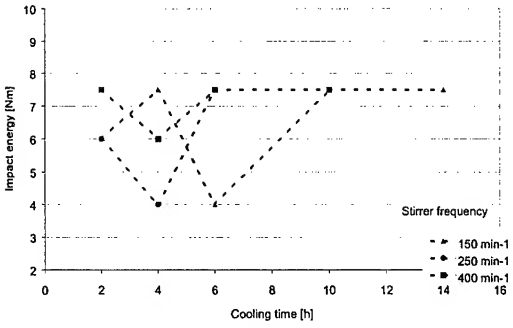

Fig. 59: Impact energy plotted versus cooling time

9.2.2 Mechanical Sensitivity / Particle Size

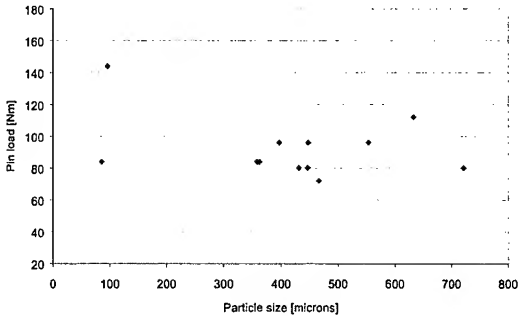

Fig. 60: Pin load plotted versus particle size

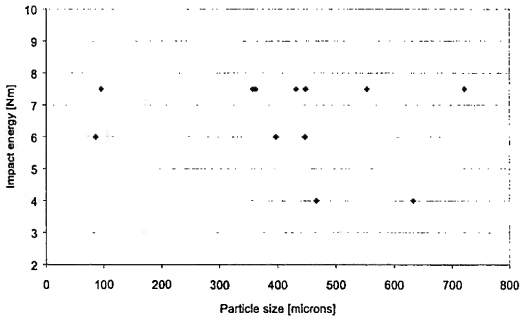

Fig. 61: Impact energy plotted versus particle size

9.2.3 Mechanical Sensitivity / Density

A significant correlation of mechanical sensitivities and measured densities was not found.

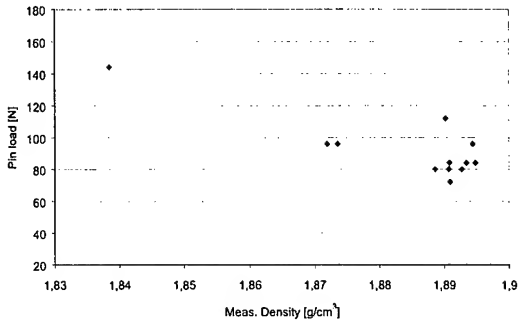

Fig. 62: Pin load plotted versus measured density

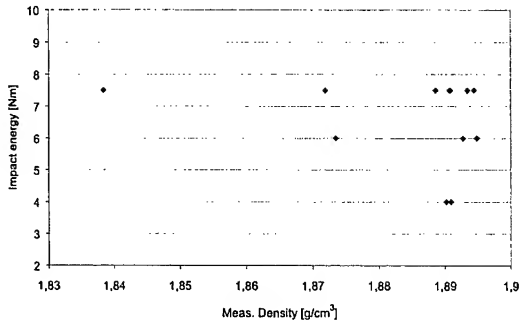

Fig. 63: Impact energy plotted versus measured density

9.2.4 Density / Crystallization Conditions

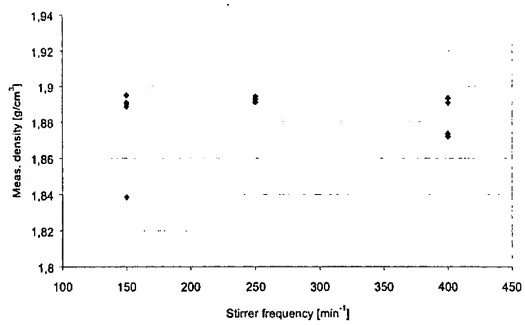

Fig. 64: Measured density plotted versus stirrer frequency

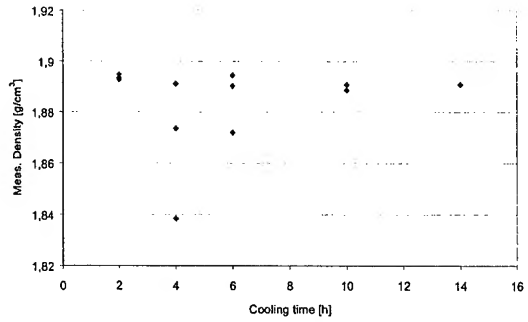

Fig. 65: Measured densities plotted versus cooling time

9.2.5 Particle Size / Crystallization parameters

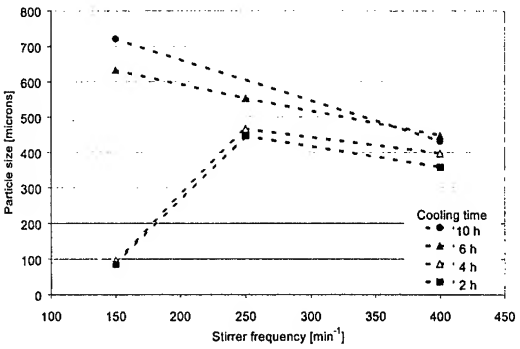

Fig. 66: Particle size plotted versus stirrer frequency

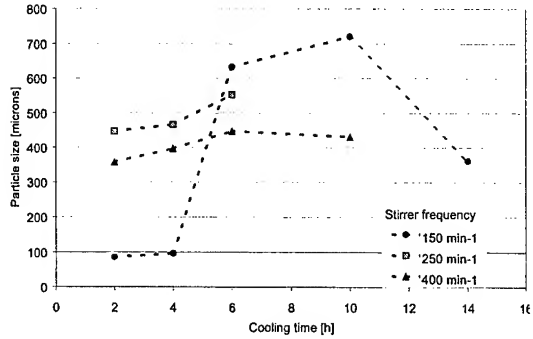

Fig. 67: Particle size plotted versus cooling time

The particle sizes of the samples plotted against stirrer frequencies and cooling rates of the crystallization are shown Fig. 66 and Fig. 67. As expected stronger stirring results in finer materials. Two unexpectedly low values, however, are obtained with the stirrer frequency of 150 min^{-1} and the cooling time 2 and 4 h. Besides, particle sizes increase with longer cooling time which was also expected, as the crystals have longer time for growing. Fig. 67 shows a maximum particle size with cooling times of 6 and 10 h and stirrer frequencies of 400 and 150 min^{-1}, respectively. The decreasing particle sizes beyond the maximum give rise for the hypothesis, that longer nucleation time result in a higher quantity of therefore smaller crystals.

9.3 Tables

Tab. 1: Conditions of the preparation of the HMX samples

Sample	Preparation	Solvent	Revolutions (turbine)	cooling rate (75-5°C)
V1	Crystallized	PC	150 / min.	2 h
V2	Crystallized	PC	150 / min.	4 h
V3	Crystallized	PC	150 / min.	6 h
V4	Crystallized	PC	250 / min.	2 h
V5	Crystallized	PC	250 / min.	4 h
V6	Crystallized	PC	250 / min.	6 h
V7	Crystallized	PC	400 / min.	2 h
V8	Crystallized	PC	400 / min.	4 h
V9	Crystallized	PC	400 / min.	6 h
V19	Crystallized	PC	150 / min.	10 h
V20	Crystallized	PC	150 / min.	14 h
V21	Crystallized	PC	400 / min.	10 h
V 42/2	Crystallized		None	
orig.	--	--	--	--
Techn.	Ground	--	--	--

PC = Propylene carbonate

Tab. 2: Peak widths of the (011)-reflection of Quartz measured with System 1, Bragg-Brentano Diffractometer, and system 2 with and Debye Scherrer device

				Slits		Peak	
		Step width	time/step	div.	antisc.	width*	intensity
No.	System	[2 Theta]	[s]	[°]	[°]	[2 Theta]	[cps]
1	D5000,	0,002	1	1	1	0,071	5212
	no rotation	0,002	1	0,1	0,1	0,059	498
		0,002	1	0,1	0,2	0,057	926
		0,002	1	0,2	0,1	0,055	898
		0,005	2,5	0,2	0,1	0,056	2172
		0,005	2,5	0,3	0,1	0,057	3166
		0,005	2,5	0,3	0,2	0,056	5433
		0,005	2,5	0,3	0,3	0,057	6877
		0,005	10	0,1	0,1	0,058	5238
2	D5000,	0,01	8,6	0,1	0,1	0,173	71
	Debye Scherrer*	0,01	8,6	0,1	0,2	0,167	73
		0,01	8,6	0,2	0,1	0,197	62
		0,01	8,6	0,2	0,1	0,175	66
		0,01	8,6	0,3	0,1	0,161	63
		0,01	8,6	1	1**	0,153	30

Detector slit = 0.6 mm, ** secondary monochromator used with slit = 0,1 mm, * FWHM

Tab. 3: Peak widths and intensities for the different measuring systems

No.	System	Sample	Reflection/Position [°2θ]	Intensity [cps]	FWHM* [°2θ]
1	D5000/D8, no sample rotation	Quartz	(011) / 26,68	500 – 7000	0,055 – 0,060**
2	D5000, Debye Scherre	Quartz	(011) / 26,68	30 – 70	0,15 – 0,2**
3	D5000, Göbel mirror	Quartz	(011) / 26,67	510 201	0,115 0,100
4	Transmission	Silicon	(111) / 28,43 (220) / 47,30	2790 1560	0,052 0,056
5	V5-cut	Silicon	(111) / 28,45 (220) / 47,30	126 42	0,028 0,038

* for details see Tab. 2, ** Full Width at Half Maximum

Tab. 4: HMX Samples measured with the different systems

No.	System	Samples
1	D5000/D8 no rotation	V1, V2, V3, V4, V5, V6, V7, V8, V9, V19, V20, V21, orig., V42/2, Techn.
4	Guinier	V2, V3, V5, V6, V9, orig., Techn.
5	V5-Cut	V2, V3, V5, V6, V9, orig., Techn.

angular range: 14 - 38 °2θ, step width: 0,005 °2θ,
measuring time: 6 s/channel = 8 h/pattern

Tab. 5: Results of the Rietveld-Analysis and Williamson-Hall-Plots

	Rietveld-Analysis System 4					Williamson Hall Plots System 1			System 4			System 5		
Probe	a	b	c	β	Dens.	m	b	R^2	m	b	R^2	m	b	R^2
V1						0,004	0,033	0,001						
V2	6,517	10,997	8,678	124,44	2,021	0,029	0,020	0,010	0,116	0,028	0,77	0,0005	0,0258	0,0001
V3	6,555	11,061	8,726	124,44	1,987	0,080	0,012	0,130	0,117	0,045	0,95	-0,015	0,0247	0,064
V4						-0,009	0,045	0,002						
V5	6,533	11,028	8,701	124,44	2,005	0,020	0,029	0,009	0,014	0,043	0,04	-0,043	0,0315	0,32
V6	6,538	11,038	8,707	124,44	2,000	0,045	0,047	0,039	0,066	0,039	0,43	-0,053	0,0315	0,25
V7	6,534	11,026	8,698	124,42	2,005	0,022	0,033	0,019	0,054	0,034	0,53	-0,062	0,0352	0,77
V8						0,064	0,020	0,119						
V9	6,53	11,028	8,694	124,42	2,007	0,037	0,031	0,068	0,074	0,035	0,42	-0,138	0,0564	0,55
V19						0,065	0,035	0,218						
V20						0,014	0,034	0,030						
V21						-0,015	0,037	0,009						
V42/2						0,015	0,034	0,005						
Techn.	6,536	11,029	8,703	124,44	2,003	0,013	0,050	0,007	0,037	0,039	0,31	0,0103	0,0393	0,03
Orig	6,537	11,032	8,701	124,42	2,002	-0,043	0,042	0,116	0,026	0,037	0,18	-0,006	0,0158	0,02

Tab. 6: Results of the investigations with the scanning electron microscope

sample	particle size				defects						eval.
	fine	min	max	mean	c. edge	u. face	holes	round.	twin	aggl.	Σ
V1	1	5	200	50	0	1	0	1	0	0	2
V2	0	10	200	50	2	1	1	0	0	1	5
V3	1	5	500	10/200	0	0	0	0	1	1	2
V4	1	5	200	50	1	1	0	1	1	1	5
V5	0	10	300	100	1	1	0	0	1	0	3
V6	0	30	500	100	1	1	0	0	1	0	3
V7	0	50	400	100	0	1	0	1	1	0	3
V8	0	30	300	100	1	1	0	0	0	1	3
V9	0	30	300	100	3	2	2	0	0	0	7
V19	2	5	200	10/200	0	0	0	0	0	1	1
V20	2	10	500		0	1	2	0	0	0	3
V21	0	10	300	80	2	1	1	1	0	0	5
V42	2	3	30	10	0	0	1	0	0	0	1
Techn.	3	1	30	5	0	3	0	3	0	2	8

c. edge = corroded edges, u. face = uneven faces, round. = rounded particles, twin = twin crystals, aggl. = agglomeration, 0 – 3 with 0 = low and 3 = high density of the defect type

Tab. 7: Particle sizes and densities of the crystallized HMX samples

sample	$x_{50,3}$ [µm]	density [g/cm³]
V1	85,5	1,895
V2	95,8	1,843
V3	632,9	1,890
V4	447	1,893
V5	466,5	1,891
V6	553,3	1,894
V7	357,9	1,893
V8	397	1,874
V9	447,8	1,872
V19	721,1	1,889
V20	362	1,891
V21	431,4	1,891

Tab. 8: Mechanical sensitivity of the HMX samples

Sample	impact test		friction test
	Weight [kg]	[Nm]	[N]*
V1	1	6,0	84
V2	5	7,5	144
V3	1	4,0	112
V4	1	6,0	80
V5	1	4,0	72
V6	5	7,5	96
V7	5	7,5	84
V8	1	6,0	96
V9	5	7,5	96
V19	5	7,5	80
V20	5	7,5	84
V21	5	7,5	80
V42/2	1	4,0	80
Techn.	1	4,0	80

* pin load